MOLECULAR AND CELLULAR BIOLOGY, Apr. 2003, p. 2556–2563 Vol. 23, No. 7
0270-7306/03/$08.00+0 DOI: 10.1128/MCB.23.7.2556–2563.2003

p53 Binding Protein 53BP1 Is Required for DNA Damage Responses and Tumor Suppression in Mice

Irene M. Ward,[1] Kay Minn,[1] Jan van Deursen,[2] and Junjie Chen[1]*

Departments of Oncology[1] and Pediatric and Adolescent Medicine,[2] Mayo Clinic and Foundation, Rochester, Minnesota 55905

Received 19 November 2002/Returned for modification 14 December 2002/Accepted 7 January 2003

53BP1 is a p53 binding protein of unknown function that binds to the central DNA-binding domain of p53. It relocates to the sites of DNA strand breaks in response to DNA damage and is a putative substrate of the ataxia telangiectasia-mutated (ATM) kinase. To study the biological role of 53BP1, we disrupted the 53BP1 gene in the mouse. We show that, similar to ATM$^{-/-}$ mice, 53BP1-deficient mice were growth retarded, immune deficient, radiation sensitive, and cancer prone. 53BP1$^{-/-}$ cells show a slight S-phase checkpoint defect and prolonged G_2/M arrest after treatment with ionizing radiation. Moreover, 53BP1$^{-/-}$ cells feature a defective DNA damage response with impaired Chk2 activation. These data indicate that 53BP1 acts downstream of ATM and upstream of Chk2 in the DNA damage response pathway and is involved in tumor suppression.

Defects in DNA damage recognition and repair mechanisms are associated with cancer predisposition. The tumor suppressor protein p53, a sequence specific transcription factor, plays a central role in the response of mammalian cells to genotoxic stress. 53BP1 (p53 binding protein 1) was cloned as a protein that interacts with the DNA-binding domain of p53 (13). It contains a tandem BRCT (BRCA1 C terminus) motif (5) with sequence homology to the tumor suppressor BRCA1 and DNA damage checkpoint protein scRad9. 53BP1 binds through the first of its C-terminal BRCT repeats and the inter-BRCT linker region to the central DNA-binding domain of p53 (7, 15) and has been shown to enhance p53-mediated transcription of reporter genes (14). More recently, in vitro studies suggest that 53BP1 participates in the cellular response to DNA damage. 53BP1 relocates to multiple nuclear foci within minutes after exposure of cells to ionizing radiation (IR) (2, 22, 23, 28). These foci colocalize with known DNA damage response proteins such as phosphorylated H2AX, Rad50/Mre11/NBS1, BRCA1, and Rad51 at sites of DNA lesions (2, 22, 23). 53BP1 becomes hyperphosphorylated in response to IR, and several lines of evidence suggest that 53BP1 is a downstream target of the ataxia telangiectasia-mutated (ATM) kinase, the product of the gene mutated in ataxia telangiectasia (2, 22, 28). Furthermore, 53BP1 localizes to kinetochores in mitotic cells, suggesting a potential function of 53BP1 in mitotic checkpoint signaling (16).

To study the biological function of 53BP1 in mammals, we created 53BP1-deficient mice. We report here that mice lacking 53BP1 are viable and display a phenotype that partially overlaps with that of ATM-deficient mice. 53BP1-deficient mice are growth retarded, immune deficient, radiation sensitive, and cancer prone. Thus, 53BP1 is required for an appropriate cellular response to DNA damage in vivo.

* Corresponding author. Mailing address: Department of Oncology, Mayo Clinic and Foundation, Rm. 1306, Guggenheim Bldg., 200 First St., SW, Rochester, MN 55905. Phone: (507) 538-1545. Fax: (507) 284-3906. E-mail: chen.junjie@mayo.edu.

MATERIALS AND METHODS

Gene targeting and generation of 53BP1-deficient mice. A mouse 53BP1 cDNA fragment was used as a probe to isolate 53BP1 mouse genomic DNA from a mouse 129 genomic DNA phage library (Stratagene). The genomic DNA was cloned into pZErO-2 (Invitrogen), and the exon-intron structure characterized by restriction digestion, Southern blotting, and DNA sequencing. The targeting vector was constructed by replacing the exon spanning nucleotides 3777 to 4048 of the mouse 53BP1 gene with the PGK-neo^r gene. The targeting vector was linearized and electroporated into 129/SvE embryonic stem (ES) cells. About 200 G418-resistant ES clones were screened by Southern blot analysis by using a probe that hybridizes to a 9.8-kb *Eco*RI restriction fragment in wild-type cells and an 8.3-kb fragment in homologous recombinants. Three independent ES clones with homologous integration at the targeting site were injected into C57BL/6 blastocysts to generate chimeric mice. These chimeras were subsequently crossed with C57BL/6 females, and heterozygous mice with successful germ line transmission of the targeted allele were used to generate 53BP1$^{-/-}$ mice.

Generation of 53BP1$^{-/-}$ MEFs and embryonic cells. Primary mouse embryonic fibroblasts (MEFs) were obtained from e14.5 embryos by a standard procedure. To generate 53BP1$^{-/-}$ embryonic cells, day 3 blastocytes from −/− matings were isolated and an embryonic cell line was established by a standard procedure.

Proliferation and clonogenic assays. MEFs from three 53BP1$^{-/-}$ and three genetically matched 53BP1$^{+/+}$ embryos were plated at a density of 10^5 cells/well in six-well plates. Every day one set of cells was treated with trypsin and counted. At days 3 and 6, cells were split and replated into larger dishes. For the clonognic cell survival assay, 53BP1$^{-/-}$ and 53BP1$^{+/+}$ embryonic cells were plated into 60-by-15-mm dishes and 6 h later exposed to different doses of IR. After 7 days of culture, the number of colonies was counted.

Western blot and immunofluorescence analysis. Western blot analyses were performed by a standard procedure. Immunofluorescence staining was performed as described previously (26). Antibodies against 53BP1, Chk2, Chk2T68P, and γ-H2AX were generated as described previously (22, 26, 27). The antibodies to p53 (FL393G) and actin were purchased from Santa Cruz and Sigma, respectively. The antibodies to mouse NBS1 and BRCA1 were gifts from A. Nussenzweig and L. Chodosh, respectively.

Cell cycle checkpoints and flow cytometry analysis. For analysis of G_2/M checkpoint function, MEFs from 53BP1$^{-/-}$ and genetically matched 53BP1$^{+/+}$ embryos, as well as ES cells, were irradiated with different doses of IR and stained 1 h later with anti-P-Histone 3 (Upstate). Aliquots of the cells were also labeled with bromodeoxyuridine (BrdU) for 1 h before exposure to 6 Gy of IR, harvested at different time points after IR, and stained with anti-BrdU-FITC (Becton Dickinson) and propidium iodide. To monitor radiation-induced inhibition of DNA synthesis, MEFs were labeled for 48 h with 20 nCi of [^{14}C]thymidine ml^{-1} before exposure to 0 or 20 Gy of IR. At 30 min after IR cells were pulse-labeled for 30 min with 2.5 mCi of [^{3}H]thymidine ml^{-1} and harvested. Radioactivity was measured in a liquid scintillation counter.

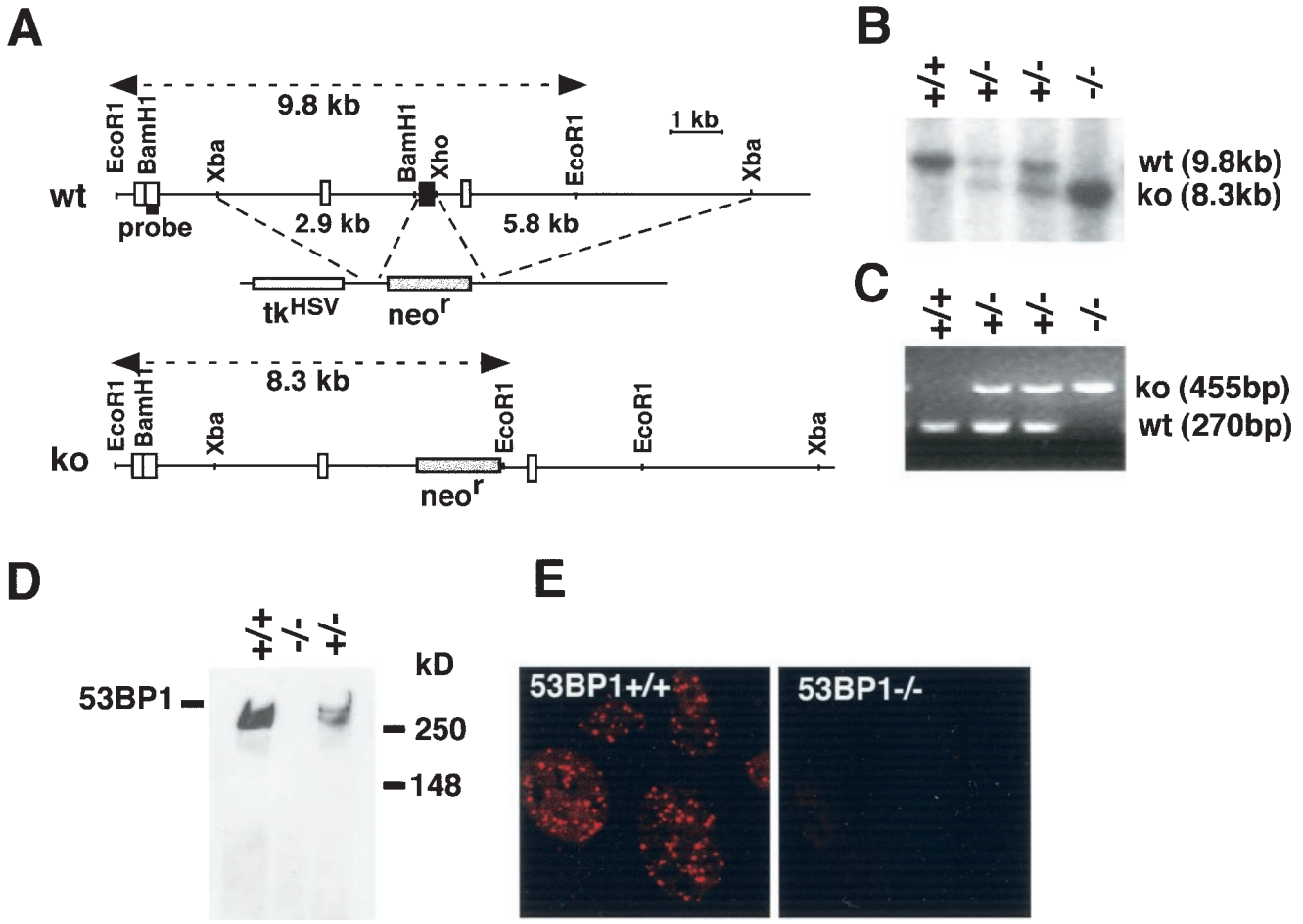

FIG. 1. Targeted disruption of the mouse 53BP1 gene. (A) Map of the genomic locus surrounding the targeted exon, the targeting vector containing the PGK-neo cassette, and the targeted locus. A 5′-flanking probe used for screening ES cell clones and mice is indicated. (B) Southern blot analysis of *Eco*RI-digested genomic DNA. (C) Multiplex PCR genotype analysis with a primer pair for the *neo* gene (resulting in a 455-bp product) and a 5′ external exon (resulting in a 270-bp product). (D) Western blot of cell extracts from mouse testes with an antibody specific for the N terminus of 53BP1. (E) Immunofluorescence analysis of irradiated (1 Gy) $53BP1^{+/+}$ and $53BP1^{-/-}$ MEFs with polyclonal antibodies raised against the N terminus of 53BP1.

Thymocytes, white blood cells, and tumor cells were stained with anti-CD4-phycoerythrin and anti-CD8-fluorescein isothiocyanate or the respective isotype controls (all from Pharmingen) and then analyzed on a flow cytometer.

Histopathological analysis and chromosome spreads. Tissues were collected and fixed in 10% buffered formalin or Bouin's fixative, embedded in paraffin blocks, sectioned, and stained with hematoxylin-eosin. Metaphase spreads were prepared by a standard procedure.

RESULTS

Phenotype of 53BP1-deficient mice. To analyze the physiological role of 53BP1 in mammalian cells, we generated 53BP1-deficient mice. The targeting vector was constructed by replacing the exon spanning nucleotides 3777 to 4048 of the mouse 53BP1 cDNA with the PGK-neo^r gene (Fig. 1A to C). $53BP1^{-/-}$ mice were viable and born at ratios close to the expected Mendelian proportion (25% [+/+], 52% [+/−], and 23% [−/−]). The complete absence of 53BP1 protein was confirmed by Western blot and immunofluorescence analyses with antibodies raised against the N terminus of 53BP1 (Fig. 1D and E).

Since 53BP1 is a putative substrate of ATM in the DNA damage response pathway, we examined whether $53BP1^{-/-}$ mice show a similar phenotype as ATM-deficient mice. $ATM^{-/-}$ mice are growth retarded and ATM-deficient fibroblasts grow poorly in culture (3, 9, 30). Similarly, $53BP1^{-/-}$ mice are significantly smaller than their +/+ and +/− littermates (male, 38.29 ± 3.6 g [+/+], 28.28 ± 3.5 g [−/−], and 34.91 ± 2.6 g [+/−]; female, 29.38 ± 4.8 g [+/+], 23.85 ± 3.1 g [−/−], and 27.89 ± 3.5g [+/−]; also see Fig. 2A). Consistent with this finding, MEFs derived from E14.5 null embryos showed a lower proliferation rate than genetically matched wild-type controls (data not shown). ATM-deficient mice are infertile due to meiotic failure (3, 9, 30). In contrast, both male and female 53BP1-deficient mice were fertile, although the average litter size of $53BP1^{-/-}$ intercrosses was slightly reduced compared to 53BP1-wild-type intercrosses (data not shown). Histological examination of the testes revealed no overt defect in spermatogenesis, suggesting that 53BP1 plays no apparent role in meiosis.

Cell cycle checkpoint regulation in $53BP1^{-/-}$ cells. ATM-deficient cells exhibit a defect in the G_2/M checkpoint and do

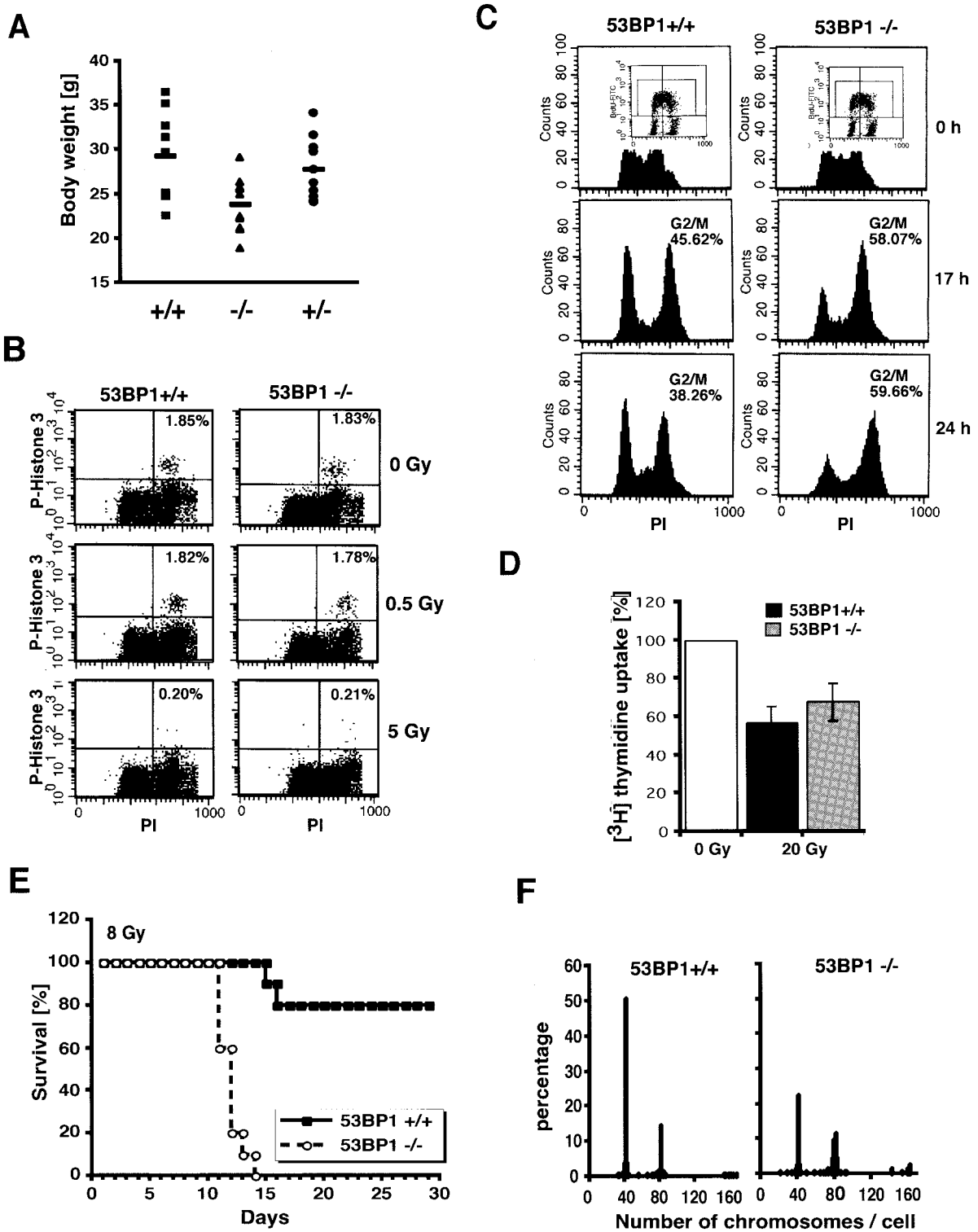

FIG. 2. 53BP1 deficiency results in growth retardation, cell cycle defect, radiosensitivity, and chromosomal instability. (A) Body weights of female 53BP1 wild-type, heterozygous, and knockout mice at 5 months of age. (B) G_2/M arrest of 53BP1$^{+/+}$ and 53BP1$^{-/-}$ embryonic cells in response to 0.5 or 5 Gy of IR. Cells were stained with anti-P-Histone 3 antibody 1 h after IR and analyzed by fluorescence-activated cell sorting. (C) G_2 accumulation of 53BP1$^{+/+}$ and 53BP1$^{-/-}$ MEFs several hours after IR. Cells were pulse-labeled for 1 h with BrdU before exposure to 6 Gy of IR. The cell cycle profile of BrdU-positive cells was analyzed by staining with propidium iodide. Consistent data were obtained in three independent experiments. (D) IR-induced intra-S-phase checkpoint in 53BP1$^{+/+}$ and 53BP1$^{-/-}$ MEFs. DNA synthesis was assessed by [3H]thymidine incorporation 30 min after exposure to 20 Gy of IR. (E) Sensitivity of 10 pairs of female 53BP1$^{-/-}$ and 53BP1$^{+/+}$ littermates to 8 Gy of whole body IR. Similar results were observed with 10 male pairs. (F) Chromosomal instability in 53BP1$^{-/-}$ MEFs. 100 metaphase spreads from genetically matched passage three 53BP1$^{+/+}$ and 53BP1$^{-/-}$ MEFs were analyzed. Consistent data were obtained from three different experiments.

not arrest in G_2 in the first 2 h after IR (for example, see reference 29). However, flow cytometric analysis of phospho-H3-positive mitotic embryonic cells revealed no apparent G_2/M checkpoint defect in 53BP1$^{-/-}$ cells in response to different doses of IR (Fig. 2B and data not shown).

Several hours after IR, ATM-deficient cells show a prolonged accumulation in G_2/M (29). A similar phenotype was observed in 53BP1$^{-/-}$ fibroblasts. As shown in Fig. 2C, irradiated 53BP1-null cells, like 53BP1$^{+/+}$ cells, were arrested in G_2 but showed a delayed exit from the G_2/M phase. Consistent with 53BP1$^{-/-}$ cells arrested at the G_2 phase, the percentage of mitotic cells 24 h after IR was approximately three times lower in nocodazole-treated 53BP1$^{-/-}$ cells than in 53BP1 wild-type cells, as assessed by immunostaining with anti-phospho-histone H3 antibodies (data not shown).

Cells derived from ataxia telangiectasia patients show a defect in the IR-induced G_1 delay (18). In contrast, 53BP1-deficient MEFs, synchronized by a cycle of serum starvation and release, exhibited a normal G_1 arrest in response to 10 to 20 Gy of IR (data not shown).

ATM-deficient cells also feature a defect in the intra-S phase checkpoint, resulting in a radioresistant DNA synthesis phenotype (3). Both 53BP1$^{+/+}$ and 53BP1$^{-/-}$ fibroblasts showed inhibition of DNA synthesis in response to 20 Gy of IR, although the response was slightly impaired in 53BP1$^{-/-}$ cells (Fig. 2D).

Thus, although 53BP1 may play a subtle role in intra-S-phase regulation, it appears not to be critical for G_1 or early G_2/M checkpoint control.

Radiosensitivity of 53BP1$^{-/-}$ mice and cells. Another hallmark of ATM-deficiency is extreme radiation sensitivity (for example, see reference 3). Similarly, 53BP1$^{-/-}$ mice showed a marked hypersensitivity to whole-body irradiation. All 53BP1$^{-/-}$ mice died by 14 days after exposure to 8 Gy of IR, whereas the majority of 53BP1$^{+/+}$ mice were viable for at least 2 months after irradiation (Fig. 2E). Necroptic examination revealed radiation-induced intestinal bleeding and bone marrow failure as the cause of death (data not shown). Consistent with this finding, in vitro clonogenic survival assays with embryonic cells indicated a two- to threefold-higher radiation sensitivity in 53BP1-deficient cells than in 53BP1-wild-type cells, although the difference was less dramatic than in vivo (data not shown).

Chromosomal instability of 53BP1$^{-/-}$ cells. To determine whether loss of 53BP1 causes chromosomal instability, another characteristic of ATM$^{-/-}$ cells, we examined metaphase spreads of passage 3 53BP1$^{-/-}$ and 53BP1$^{+/+}$ MEFs. Unlike ATM-deficient cells, 53BP1$^{-/-}$ fibroblasts showed no spontaneous chromosomal breaks. However, we observed a tendency toward aneuploidy and/or tetraploidy in 53BP1-null cells, suggesting a possible defect in chromosome segregation (Fig. 2F).

Immunodeficiency and thymic lymphomas in 53BP1$^{-/-}$ mice. ATM$^{-/-}$ mice show various immune defects, including reduced numbers of pre-B cells, thymocytes, and peripheral T cells, and develop malignant thymic lymphomas by between 2 and 4 months of age (3, 9, 30). We therefore sought to determine whether the loss of 53BP1 might be accompanied by immunological abnormalities and predisposition to tumor formation. Indeed, thymus cellularity in 53BP1$^{-/-}$ mice was reduced by 40% compared to wild-type littermates. Immunophenotyping of 6-week-old mice revealed an approximately twofold reduction in the percentage of CD4$^+$ mature thymocytes (with absolute average numbers of 7×10^6 cells in 53BP1$^{+/+}$ mice and 2.8×10^6 cells in 53BP1$^{-/-}$ mice) accompanied by a maximum twofold increase in the percentage of CD4$^-$ CD8$^-$ progenitors. CD4$^+$ T lymphocytes in the peripheral blood of 53BP1$^{-/-}$ mice were also reduced by approximately twofold (with absolute average numbers of 8.2×10^5 cells/ml in 53BP1$^{-/-}$ mice and 16.9×10^5 cells/ml in 53BP1$^{+/+}$ mice). Furthermore, of 101 53BP1$^{-/-}$ mice, 8 developed massive thymic lymphomas with or without infiltration of the lymph nodes, spleen, and kidney at the ages of 4 to 7 months (Fig. 3A to C). Flow cytometric analysis of three of these tumors revealed a CD4$^+$ CD8$^+$ immunophenotype (Fig. 3A and data not shown). Although the tumor frequency in 53BP1$^{-/-}$ mice is much lower than in ATM$^{-/-}$ mice (8% versus 100%), it is highly significant since none of the 53BP1$^{+/+}$ and 53BP1$^{+/-}$ mice ($n = 54$ and $n = 97$, respectively) developed any tumors over the same time period. In addition to the eight 53BP1$^{-/-}$ mice with malignant lymphomas, nine more 53BP1$^{-/-}$ mice died at the ages of 1 to 7 months without overt detectable tumors (Fig. 3D). Given the chronic immunosuppression of 53BP1$^{-/-}$ mice, it is possible that some of these deaths might be due to overwhelming opportunistic infections. Among the control animals, only one 53BP1$^{+/+}$ mouse and two 53BP1$^{+/-}$ miced died of unidentified reasons (Fig. 3D).

Role of 53BP1 in DNA damage signaling pathway. The partially overlapping phenotypes of 53BP1- and ATM-deficient mice support the hypothesis that 53BP1 acts downstream of ATM in the DNA damage pathway. ATM becomes activated in response to irradiation and phosphorylates numerous downstream targets, including H2AX, NBS1, Chk2, and p53, that mediate cell cycle checkpoint control and DNA repair (for example, see reference 1). To obtain a better understanding of the complex organization of this pathway, we examined the effect of 53BP1 deficiency on the activation of some of these downstream targets.

We have shown earlier that 53BP1 associates with γ-H2AX within minutes after exposure to IR (22), thus raising the possibility that γ-H2AX may be required for the recruitment of 53BP1. Indeed, 53BP1 foci are not observed in H2AX-deficient cells (6). Consistent with this model, γ-H2AX foci formation was found normal in 53BP1$^{-/-}$ MEFs (Fig. 4A), suggesting that 53BP1 acts downstream of ATM and H2AX. Since H2AX is also required for the localization of NBS1 to the sites of DNA breaks (6, 21), we examined whether any of these events are 53BP1 dependent. As shown in Fig. 4A, radiation-induced NBS1 foci formation appears to be normal in 53BP1$^{-/-}$ cells, suggesting that 53BP1 is not required for the recruitment of NBS1 to sites of DNA strand breaks.

Chk2 is another downstream effector of ATM. Chk2 is activated after IR and contributes to the IR-induced checkpoint control by phosphorylating several substrates including Cdc25C, Cdc25A, BRCA1, and p53 (4). ATM phosphorylates Chk2 at Thr-68 in response to IR, and this phosphorylation event is required for the full activation of Chk2 kinase (19, 20). Coimmunoprecipitation analyses demonstrate an interaction between 53BP1 and Chk2 in undam-

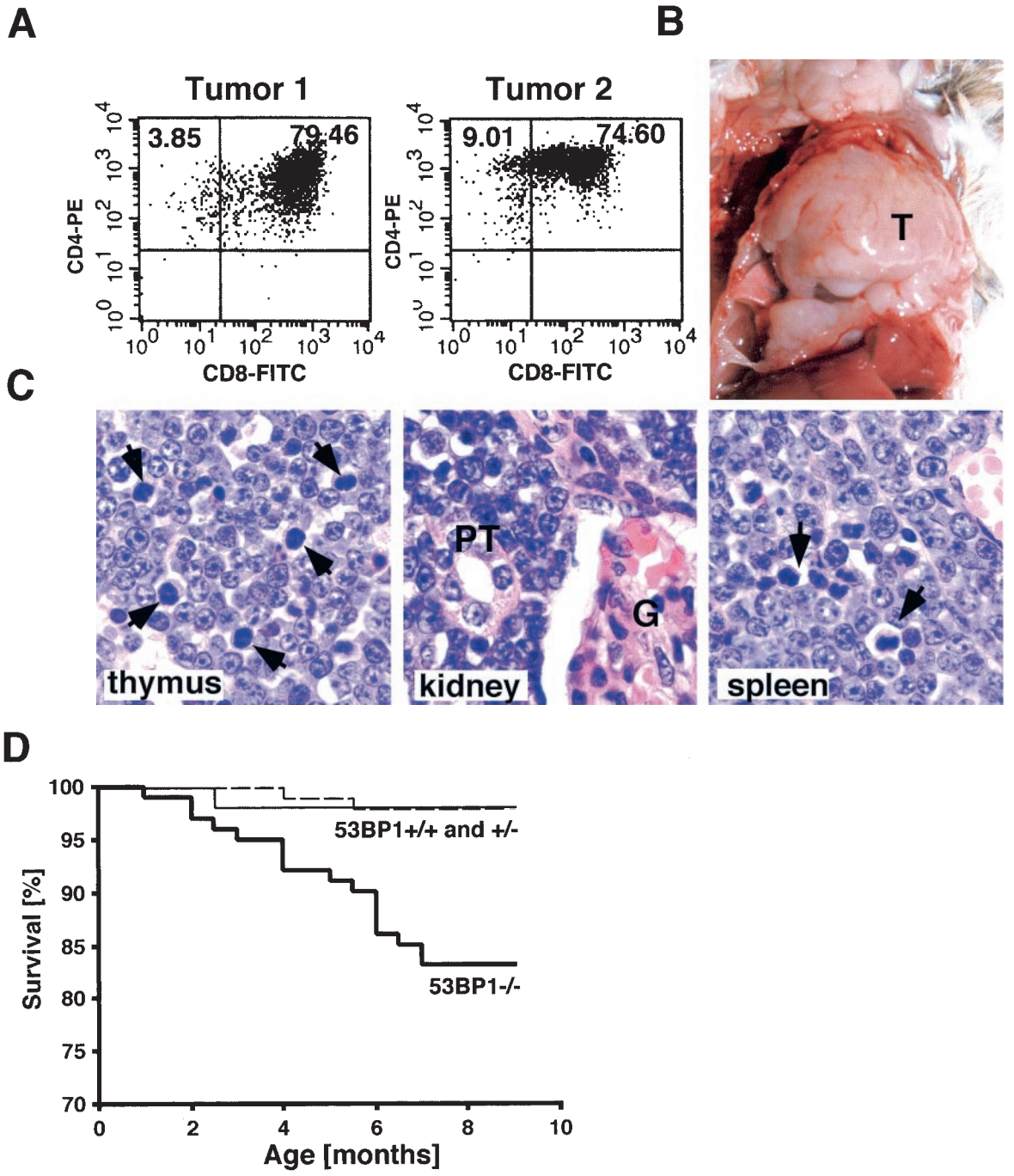

FIG. 3. 53BP1$^{-/-}$ mice are tumor prone. (A) CD4 and CD8 cell surface expression of cells from two different thymic lymphomas was assessed by flow cytometry. (B) Massive thymic lymphoma (T) in a 4-month-old 53BP1$^{-/-}$ mouse. (C) Hematoxylin-and-eosin-stained sections from the thymus, spleen, and kidney of a 53BP1$^{-/-}$ animal with thymic lymphoma. Monomorphic lymphoblastic tumor cells are dominant in all three tissues. The arrows indicate mitotic figures. G, glomerulus; PT, proximal tubulus. (D) Overall survival of 53BP1$^{+/+}$ (n = 54), 53BP1$^{+/-}$ (n = 97), and 53BP1$^{-/-}$ (n = 101) mice over a period of 10 months.

aged cells (Fig. 4B). Interestingly, this interaction decreases after IR (Fig. 4B). Since we have shown earlier that the activated form of Chk2 localizes in distinct foci at the sites of DNA lesions (27), we first examined the focus formation of phospho-Chk2. In these experiments, we used a guinea pig anti-Chk2T68P antibody that specifically recognizes Chk2 in Chk2$^{+/+}$ cells but not in Chk2$^{-/-}$ cells (Fig. 4G). As shown in Fig. 4C, focus formation of phosphorylated Chk2 (Chk2T68P) was abolished in 53BP1$^{-/-}$ MEFs upon exposure to 1 Gy of IR. Furthermore, Chk2 phosphorylation, as assessed by gel mobility shift, was reduced in 53BP1$^{-/-}$ MEFs in response to low doses of radiation (≤5 Gy, Fig. 4E

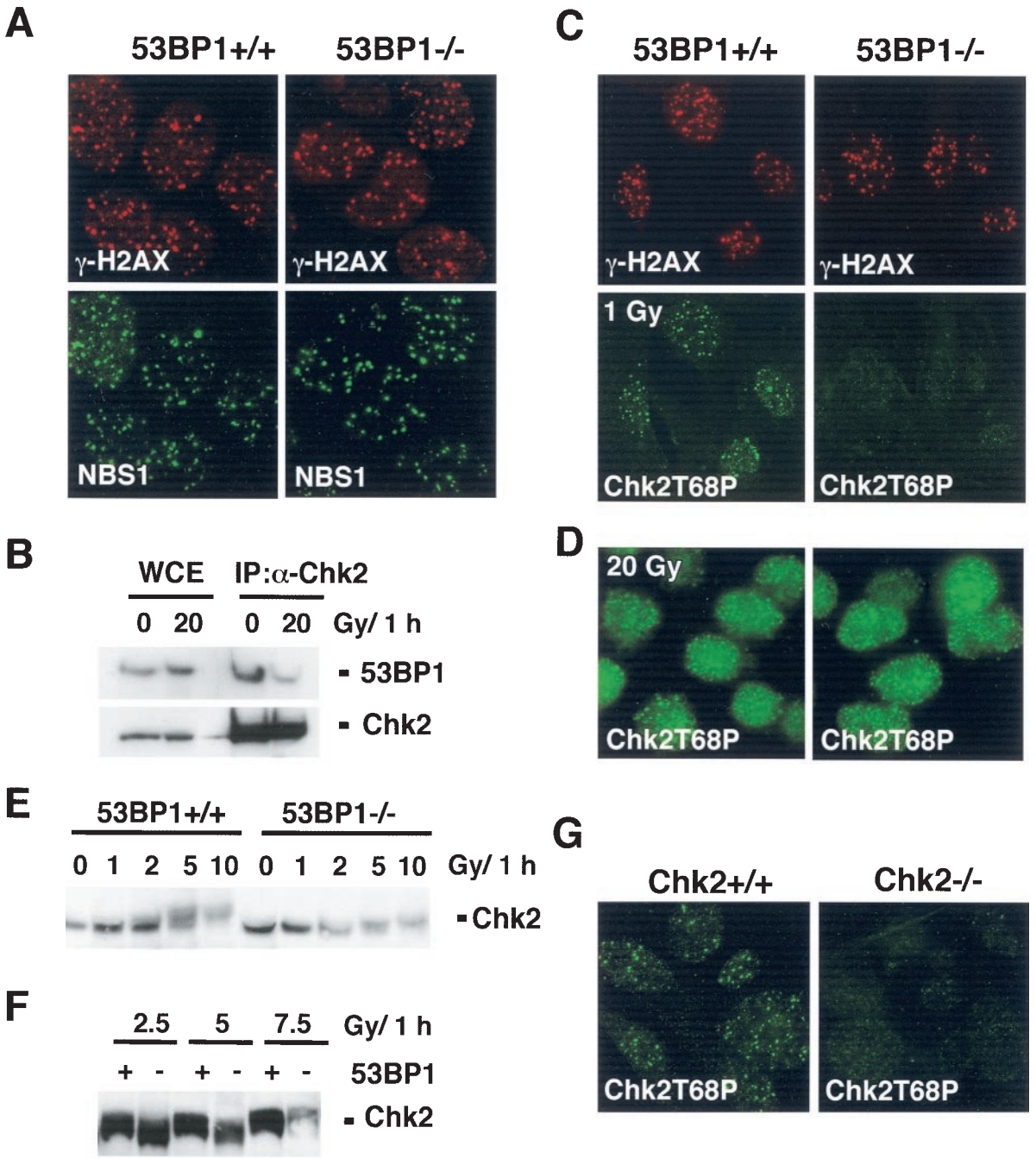

FIG. 4. Irradiated 53BP$^{-/-}$ MEFs show impaired Chk2 activation after low doses of IR. (A) γ-H2AX and NBS1 focus formation 6 h after exposure to 6 Gy of IR is unaffected in 53BP1$^{-/-}$MEFs compared to 53BP1 wild-type MEFs, as assessed by immunofluorescence staining. (B) Coimmunoprecipitation of 53BP1 and Chk2 in untreated or irradiated 293T cells. (C) Activated Chk2 phosphorylated at Thr 68 (Chk2T68) forms foci in 53BP1$^{+/+}$ MEFs 1 h after exposure to 1 Gy of IR. No foci are detectable in 53BP1$^{-/-}$ MEFs at this low dose of IR. γ-H2AX staining is shown as a control. (D) Chk2T68P foci form in both 53BP1$^{+/+}$ and 53BP1$^{-/-}$ cells in response to 20 Gy of IR. (E) Chk2 mobility shift is reduced in 53BP1$^{-/-}$ MEFs in response to low-dose radiation. Cell lysates from 53BP1$^{+/+}$ and 53BP1$^{-/-}$ MEFs were prepared 1 h after IR and immunoblotted with anti-Chk2 antibody. (F) For better comparison of the Chk2 mobility shift, lysates from irradiated 53BP1$^{+/+}$ and 53BP1$^{-/-}$ cells were run side by side. (G) The guinea pig anti-Chk2T68P antibody specifically recognizes Chk2.

and F). However, no difference in Chk2T68 focus formation or Chk2 mobility shift was observed at high doses of IR (Fig. 4D and F and data not shown). These findings suggest that 53BP1 is required for optimal activation of Chk2 after low doses of IR.

DISCUSSION

By disrupting the 53BP1 gene, we generated mice that lack 53BP1 protein. 53BP1-deficient mice are growth retarded, immunocompromised, and highly radiation sensitive. Further-

more, 8 of 101 53BP1$^{-/-}$ mice developed lymphoid tumors at 4 to 7 months of age. Cells derived from 53BP1-deficient mice show a tendency to genetic instability and feature a defective DNA damage response with impaired Chk2 activation. Thus, 53BP1 is likely to be required for the cellular response to DNA damage, although its precise role remains to be resolved.

We did not observe any marked cell cycle checkpoint defects in 53BP1-deficient cells. B cells from 53BP1$^{-/-}$ mice (11), as well as human cell lines treated with small interfering RNA directed against 53BP1, show an impaired early G_2M checkpoint in response to low-dose IR (25). However, we failed to detect this defect in 53BP1$^{-/-}$ mouse embryonic cells. This discrepancy may be due to tissue-specific functions of 53BP1 since the experiments were performed with different types of cells or cell lines. Similarly, H2AX$^{-/-}$ B cells show a clearly impaired early G_2M checkpoint, whereas the defect is very minor in H2AX$^{-/-}$ MEFs (11).

The prolonged G_2 arrest observed several hours after exposure to IR is unlikely to represent a checkpoint defect but rather reflects an impaired ability to repair DNA double-strand breaks (DSBs) prior to progressing through the cell cycle. This idea is supported by the hypersensitivity of 53BP1-deficient mice to IR. Mammalian cells are thought to repair DNA DSBs primarily by nonhomologous end joining (17). Homologous recombination, the predominant DSB repair pathway in bacteria and yeast, appears to have a minor contribution to the repair of IR in adult mice, although it plays a major role during DNA replication in embryos (10). The IR hypersensitivity observed in adult 53BP1$^{-/-}$ mice, together with a moderate IR sensitivity seen in embryonic cells, points to a defect in the DNA end-joining pathway. However, further experiments need to be conducted to resolve the precise repair defects in 53BP1-deficient cells.

One important function of DNA end joining lies in the processing of RAG1/2-induced DSBs that arise during the rearrangement of V(D)J segments in T-cell receptor and immunoglobulin genes (10). Unrepaired RAG-induced DSBs can initiate translocations that lead to oncogenic gene amplification and transformation (8, 31). 53BP1-deficient mice exhibit immunological abnormalities and an increased risk of developing lymphomas. We speculate that 53BP1$^{-/-}$ lymphomas arise from an inability to detect or repair abnormal V(D)J recombination, although further studies are necessary to clarify the underlying mechanism of lymphoma development in 53BP1-deficient mice.

53BP1-deficient cells exhibit a defect in Chk2 activation in response to low-dose IR. Interestingly, the phenotype of Chk2$^{-/-}$ mice is very different from that of 53BP1$^{-/-}$ mice. Chk2-deficient mice show reduced sensitivity to IR, and Chk2$^{-/-}$ thymocytes exhibit resistance to IR-induced apoptosis (12, 24). In contrast, 53BP1$^{-/-}$ mice are IR hypersensitive and 53BP1$^{-/-}$ thymocytes show increased IR-induced apoptosis (unpublished observations). These differences indicate that the phenotype of 53BP1-deficient mice or cells is not primarily mediated by Chk2, although 53BP1 is required for optimal Chk2 activation in response to low-dose IR.

Taken together, our data demonstrate that 53BP1 plays a role early in the DNA damage response pathway. 53BP1 acts downstream of ATM and H2AX and participates in a subset of ATM functions. 53BP1 is required for optimal activation of Chk2 in response to low doses of IR. More importantly, loss of 53BP1 leads to radiation sensitivity and tumorigenesis in mice, further supporting the hypothesis that defects in DNA damage responses contribute to tumorigenesis in mammals.

ACKNOWLEDGMENTS

We thank Andre Nussenzweig, Lewis Chodosh, Xiaohua Wu, Shirdar Ganesan, and David Livingston for valuable reagents and Larry Karnitz, Scott Kaufmann, and members of the Chen and Karnitz laboratories for helpful discussions. We are grateful to the Mayo Protein Core facility for synthesis of peptides and the Mayo Monoclonal Core facility for help in antibody production.

This work was supported by grants from National Institute of Health, the Breast Cancer Research Foundation, and Prospect Creek Foundation. J.C. is a recipient of DOD breast cancer career development award. I.W. is supported by a postdoctoral fellowship from the DOD Breast Cancer Research program.

REFERENCES

1. **Abraham, R. T.** 2001. Cell cycle checkpoint signaling through the ATM and ATR kinases. Genes Dev. **15:**2177–2196.
2. **Anderson, L., C. Henderson, and Y. Adachi.** 2001. Phosphorylation and rapid relocalization of 53BP1 to nuclear foci upon DNA damage. Mol. Cell. Biol. **21:**1719–1729.
3. **Barlow, C., S. Hirotsune, R. Paylor, M. Liyanage, M. Eckhaus, F. Collins, Y. Shiloh, J. N. Crawley, T. Ried, D. Tagle, and A. Wynshaw-Boris.** 1996. ATM-deficient mice: a paradigm of ataxia telangiectasia. Cell **86:**159–171.
4. **Bartek, J., J. Falck, and J. Lukas.** 2001. CHK2 kinase: a busy messenger. Nat. Rev. Mol. Cell. Biol. **2:**877–886.
5. **Callebaut, I., and J. P. Mornon.** 1997. From BRCA1 to RAP1: a widespread BRCT module closely associated with DNA repair. FEBS Lett. **400:**25–30.
6. **Celeste, A., S. Petersen, P. J. Romanienko, O. Fernandez-Capetillo, H. T. Chen, O. A. Sedelnikova, B. Reina-San-Martin, V. Coppola, E. Meffre, M. J. Difilippantonio, C. Redon, D. R. Pilch, A. Olaru, M. Eckhaus, R. D. Camerini-Otero, L. Tessarollo, F. Livak, K. Manova, W. M. Bonner, M. C. Nussenzweig, and A. Nussenzweig.** 2002. Genomic instability in mice lacking histone H2AX. Science **296:**922–927.
7. **Derbyshire, D. J., B. P. Basu, L. C. Serpell, W. S. Joo, T. Date, K. Iwabuchi, and A. J. Doherty.** 2002. Crystal structure of human 53BP1 BRCT domains bound to p53 tumour suppressor. EMBO J. **21:**3863–3872.
8. **Difilippantonio, M. J., S. Petersen, H. T. Chen, R. Johnson, M. Jasin, R. Kanaar, T. Ried, and A. Nussenzweig.** 2002. Evidence for replicative repair of DNA double-strand breaks leading to oncogenic translocation and gene amplification. J. Exp. Med. **196:**469–480.
9. **Elson, A., Y. Wang, C. J. Daugherty, C. C. Morton, F. Zhou, J. Campos-Torres, and P. Leder.** 1996. Pleiotropic defects in ataxia-telangiectasia protein-deficient mice. Proc. Natl. Acad. Sci. USA **93:**13084–13089.
10. **Essers, J., H. van Steeg, J. de Wit, S. M. Swagemakers, M. Vermeij, J. H. Hoeijmakers, and R. Kanaar.** 2000. Homologous and non-homologous recombination differentially affect DNA damage repair in mice. EMBO J. **19:**1703–1710.
11. **Fernandez-Capetillo, O., H. T. Chen, A. Celeste, I. Ward, P. J. Romanienko, J. C. Morales, K. Naka, Z. Xia, R. D. Camerini-Otero, N. Motoyama, P. B. Carpenter, W. M. Bonner, J. Chen, and A. Nussenzweig.** 2002. DNA damage-induced G_2-M checkpoint activation by histone H2AX and 53BP1. Nat. Cell Biol. **4:**993–997.
12. **Hirao, A., A. Cheung, G. Duncan, P. M. Girard, A. J. Elia, A. Wakeham, H. Okada, T. Sarkissian, J. A. Wong, T. Sakai, E. De Stanchina, R. G. Bristow, T. Suda, S. W. Lowe, P. A. Jeggo, S. J. Elledge, and T. W. Mak.** 2002. Chk2 is a tumor suppressor that regulates apoptosis in both an ataxia telangiectasia mutated (ATM)-dependent and an ATM-independent manner. Mol. Cell. Biol. **22:**6521–6532.
13. **Iwabuchi, K., P. L. Bartel, B. Li, R. Marraccino, and S. Fields.** 1994. Two cellular proteins that bind to wild-type but not mutant p53. Proc. Natl. Acad. Sci. USA **91:**6098–6102.
14. **Iwabuchi, K., B. Li, H. F. Massa, B. J. Trask, T. Date, and S. Fields.** 1998. Stimulation of p53-mediated transcriptional activation by the p53-binding proteins, 53BP1 and 53BP2. J. Biol. Chem. **273:**26061–26068.
15. **Joo, W. S., P. D. Jeffrey, S. B. Cantor, M. S. Finnin, D. M. Livingston, and N. P. Pavletich.** 2002. Structure of the 53BP1 BRCT region bound to p53 and its comparison to the Brca1 BRCT structure. Genes Dev. **16:**583–593.
16. **Jullien, D., P. Vagnarelli, W. C. Earnshaw, and Y. Adachi.** 2002. Kinetochore localisation of the DNA damage response component 53BP1 during mitosis. J. Cell Sci. **115:**71–79.
17. **Kanaar, R., J. H. Hoeijmakers, and D. C. van Gent.** 1998. Molecular mechanisms of DNA double strand break repair. Trends Cell Biol. **8:**483–489.
18. **Khanna, K. K., H. Beamish, J. Yan, K. Hobson, R. Williams, I. Dunn, and**

M. F. Lavin. 1995. Nature of G_1/S cell cycle checkpoint defect in ataxia-telangiectasia. Oncogene **11:**609–618.
19. **Matsuoka, S., G. Rotman, A. Ogawa, Y. Shiloh, K. Tamai, and S. J. Elledge.** 2000. Ataxia telangiectasia-mutated phosphorylates Chk2 in vivo and in vitro. Proc. Natl. Acad. Sci. USA **97:**10389–10394.
20. **Melchionna, R., X. B. Chen, A. Blasina, and C. H. McGowan.** 2000. Threonine 68 is required for radiation-induced phosphorylation and activation of Cds1. Nat. Cell Biol. **2:**762–765.
21. **Paull, T. T., E. P. Rogakou, V. Yamazaki, C. U. Kirchgessner, M. Gellert, and W. M. Bonner.** 2000. A critical role for histone H2AX in recruitment of repair factors to nuclear foci after DNA damage. Curr. Biol. **10:**886–895.
22. **Rappold, I., K. Iwabuchi, T. Date, and J. Chen.** 2001. Tumor suppressor p53 binding protein 1 (53BP1) is involved in DNA damage-signaling pathways. J. Cell Biol. **153:**613–620.
23. **Schultz, L. B., N. H. Chehab, A. Malikzay, and T. D. Halazonetis.** 2000. p53 binding protein 1 (53BP1) is an early participant in the cellular response to DNA double-strand breaks. J. Cell Biol. **151:**1381–1390.
24. **Takai, H., K. Naka, Y. Okada, M. Watanabe, N. Harada, S. Saito, C. W. Anderson, E. Appella, M. Nakanishi, H. Suzuki, K. Nagashima, H. Sawa, K. Ikeda, and N. Motoyama.** 2002. Chk2-deficient mice exhibit radioresistance and defective p53-mediated transcription. EMBO J. **21:**5195–5205.
25. **Wang, B., S. Matsuoka, P. B. Carpenter, and S. J. Elledge.** 2002. 53BP1, a mediator of the DNA damage checkpoint. Science **283:**1435–1438.
26. **Ward, I. M., and J. Chen.** 2001. Histone H2AX is phosphorylated in an ATR-dependent manner in response to replicational stress. J. Biol. Chem. **276:**47759–47762.
27. **Ward, I. M., X. Wu, and J. Chen.** 2001. Threonine 68 of Chk2 is phosphorylated at sites of DNA strand breaks. J. Biol. Chem. **276:**47755–47758.
28. **Xia, Z., J. C. Morales, W. G. Dunphy, and P. B. Carpenter.** 2001. Negative cell cycle regulation and DNA damage inducible phosphorylation of the BRCT protein 53BP1. J. Biol. Chem. **276:**2708–2718.
29. **Xu, B., S. T. Kim, D. S. Lim, and M. B. Kastan.** 2002. Two molecularly distinct G_2/M checkpoints are induced by ionizing irradiation. Mol. Cell. Biol. **22:**1049–1059.
30. **Xu, Y., T. Ashley, E. E. Brainerd, R. T. Bronson, M. S. Meyn, and D. Baltimore.** 1996. Targeted disruption of ATM leads to growth retardation, chromosomal fragmentation during meiosis, immune defects, and thymic lymphoma. Genes Dev. **10:**2411–2422.
31. **Zhu, C., K. D. Mills, D. O. Ferguson, C. Lee, J. Manis, J. Fleming, Y. Gao, C. C. Morton, and F. W. Alt.** 2002. Unrepaired DNA breaks in p53-deficient cells lead to oncogenic gene amplification subsequent to translocations. Cell **109:**811–821.